

# Recombination energy in double white dwarf formation

J.L.A. Nandez<sup>1\*</sup>, N. Ivanova<sup>1</sup>, and J.C. Lombardi Jr.<sup>2</sup>

<sup>1</sup>*Department of Physics, University of Alberta, Edmonton, AB, T6G 2E7, Canada*

<sup>2</sup>*Department of Physics, Allegheny College, Meadville, PA 16335, USA*

Draft date: 11 March 2015

## ABSTRACT

In this *Letter* we investigate the role of recombination energy during a common envelope event. We confirm that taking this energy into account helps to avoid the formation of the circumbinary envelope commonly found in previous studies. For the first time, we can model a complete common envelope event, with a clean compact double white dwarf binary system formed at the end. The resulting binary orbit is almost perfectly circular. In addition to considering recombination energy, we also show that between 1/4 and 1/2 of the released orbital energy is taken away by the ejected material. We apply this new method to the case of the double-white dwarf system WD 1101+364, and we find that the progenitor system at the start of the common envelope event consisted of a  $\sim 1.5M_{\odot}$  red giant star in a  $\sim 30$  day orbit with a white dwarf companion.

**Key words:** white dwarfs – hydrodynamic – equation of state – binaries: close

## 1 INTRODUCTION

The formation of a compact binary system composed of two white dwarfs (WDs) is widely accepted to include a common envelope event (CEE), at least during the last episode of mass exchange between the first-formed WD and a low-mass red giant (RG). Low-mass RGs have a well-defined relation between their core masses and radii, providing for DWDs the best-defined state of a progenitor binary system at the onset of the CEE among all known types of post-common envelope (CE) systems. As a result, DWD systems have served extensively as test-sites for attempts to understand the physics of CEEs, using both population synthesis approaches and hydrodynamical methods.

Previous attempts to model a CEE between a low-mass RG and a WD did not succeed to eject the entire CE during three-dimensional (3D) hydrodynamical simulations (for most recent studies, see Passy et al. 2012; Ricker & Taam 2012). The final state of these simulations is that a significant fraction of the expanded envelope remains bound to the formed binary, forming a so-called circumbinary envelope. Then almost no energy transfer can take place from the binary orbit to that circumbinary envelope. Observationally, no circumbinary disk in a post-common envelope system has been found so far.

It has been proposed long ago that recombination energy of hydrogen and helium should play a role during a CEE (Lucy 1967; Roxburgh 1967; Paczyński & Ziółkowski 1968; Han et al. 1994, 2002). However, until now, this energy was not yet taken into account in 3D modeling. While the initially available recombination energy can be easily comparable to the binding energy of the remaining bound envelope (e.g. Passy et al. 2012), the important

question is *when and where* the energy is released – to be useful, recombination energy should not be released too early in the CEE nor in material already ejected, but instead in the circumbinary envelope at a time when the recombination energy is comparable to the binding energy of the not-yet ejected material. In this *Letter*, we investigate if the inclusion of recombination energy can help to remove the circumbinary envelope. We apply the new approach to the system WD 1101+364, a well-measured DWD that has  $P_{\text{orb}} = 0.145$  d and a mass ratio of  $q = M_1/M_2 = 0.87 \pm 0.03$ , where  $M_1 \simeq 0.31M_{\odot}$  and  $M_2 \simeq 0.36M_{\odot}$  are the masses of the younger and older WDs, respectively (Marsh 1995).

## 2 INITIAL SET UP AND DEFINITIONS

We anticipate that the progenitor of WD 1101+364 was a low-mass RG that had a degenerate core of  $0.31M_{\odot}$ . We consider the range of masses for the RG donor,  $M_{\text{d},1}$ , from  $1.0M_{\odot}$  to  $1.8M_{\odot}$ . To evolve the RG and find the initial one-dimensional (1D) stellar profile, we use *TWIN/Star* stellar code (recent updates described in Glebbeek et al. 2008). The stars are evolved until their degenerate He cores have grown close to  $0.31M_{\odot}$ .

For 3D simulations, we use *StarSmasher* (Gaburov et al. 2010; Lombardi et al. 2011), a Smoothed Particle Hydrodynamics (SPH) code. Technical details on using this code to treat CE events can be found in Nandez et al. (2014). A 1D stellar profile is imported to *StarSmasher*, where an initial stellar model represented by a certain number of particles  $N_p$  is generated via a *relaxation* process. The core of a RG is modeled as a point mass – a special particle in SPH that interacts only gravitationally with other particles. Because the centre of the giant is not fully resolved, the core mass,  $M_{\text{c},1}$ , is slightly more than in the 1D code (see Table

\* E-mail: avendaon@ualberta.ca (JLAN)

**Table 1.** Initial conditions

Model	$M_{d,1}$	$M_{env,1}$	$M_{c,1}$	$R_{\text{rlf}}$	$a_{\text{orb,ini}}$	$P_{\text{orb,ini}}$	$N_p$	$\eta$	$E_{\text{bind}}$	$E_{\text{rec}}$	$E_{\text{orb,ini}}$	$E_{\text{tot,ini}}$	$\lambda$
1.0RG0N	0.985	0.668	0.317	28.21	60.11	46.57	99955	0.00	-8.454	2.059	-1.118	-7.513	1.047
1.0RG1N	0.985	0.668	0.317	29.78	63.51	50.57	99955	1.00	-8.454	2.059	-1.058	-7.453	0.992
1.0RG2N	0.985	0.668	0.317	31.35	66.81	54.57	99955	2.00	-8.454	2.059	-1.006	-7.401	0.942
1.2RG2N	1.195	0.877	0.318	29.48	60.74	44.00	99955	2.00	-12.328	2.725	-1.345	-10.945	1.093
1.4RG2N	1.397	1.079	0.319	27.73	55.59	36.24	99955	2.00	-16.947	3.369	-1.715	-15.293	1.217
1.5RG2N	1.498	1.179	0.319	25.66	50.82	30.81	99955	1.65	-20.636	4.038	-2.015	-18.609	1.267
1.5RG2NP	1.498	1.179	0.318	25.66	50.82	30.81	200221	1.65	-20.345	3.697	-2.011	-18.659	1.285
1.6RG2N	1.598	1.275	0.323	25.80	50.54	29.76	99955	2.00	-22.837	4.009	-2.157	-20.985	1.312
1.6RG0S	1.598	1.275	0.323	31.25	48.61	27.97	99955	0.00	-22.358	3.997	-2.241	-20.602	1.106
1.7RG2N	1.699	1.376	0.323	22.83	44.25	23.78	99955	2.00	-28.638	4.338	-2.619	-26.918	1.356
1.7RG0S	1.699	1.376	0.323	27.58	42.97	22.67	99955	0.00	-28.003	4.326	-2.694	-26.371	1.148
1.8RG2N	1.799	1.481	0.318	16.34	31.37	13.86	99955	2.00	-44.167	4.676	-3.912	-43.404	1.401

The models names are composed as following: two digits representing the RG mass are followed by “RG”,  $\eta$  value is is outermost smoothing length; then “N” stands for non-synchronized and “S” for synchronized (“S”) cases. “P” denotes the model with about twice larger number of particles than in all the other models.  $M_{d,1}$ ,  $M_{env,1}$  and  $M_{c,1}$  are the total, envelope and core mass of the RG, in  $M_\odot$ .  $R_{\text{rlf}}$  is the radius of the donor Roche lobe, in  $R_\odot$ , and  $\eta$  describes the adopted donor’s radius definition (see §2).  $a_{\text{orb,ini}}$  is the initial orbital separation in  $R_\odot$ ,  $P_{\text{orb,ini}}$  is the initial orbital period in days.  $N_p$  is the total number of SPH particles that represent the RG.  $E_{\text{bind}}$ ,  $E_{\text{rec}}$ ,  $E_{\text{orb,ini}}$  and  $E_{\text{tot,ini}}$  are the binding energy of the RG envelope without recombination energy, the total recombination energy of the RG envelope, initial orbital energy, and initial total energy, defined as the sum of the binding, recombination, and initial orbital energies, respectively, in the units of  $10^{46}$  erg.  $\lambda$  is a star structure parameter (see Equation 3).

1 for this and other initial values). This ensures a proper matching of stellar profiles of 3D envelopes with 1D stellar profiles. The envelope mass in a 3D star is  $M_{\text{env},1} = M_{d,1} - M_{c,1}$ .

In a 3D star, the radius of the star,  $R_{\text{SPH}}$ , can not be defined as uniquely as the photospheric radius of the 1D star (for a thorough discussion, see Nandez et al. 2014). The stellar radius can be parameterized as  $R_{\text{SPH}} = R_{\text{out}} + \eta h_{\text{out}}$ , where  $R_{\text{out}}$  is the position of the outermost particle and  $h_{\text{out}}$  is the smoothing length of that particle. The parameter  $\eta$  can range between 0 (in this case, some mass will be found above  $R_{\text{SPH}}$ ) to 2 (with all mass contained within  $R_{\text{SPH}}$ ). In addition, we note that a synchronized giant is expected to attain a larger radius after relaxation than a non-synchronized giant.

The initial orbital separation,  $a_{\text{orb,ini}}$ , for the non-synchronized cases, is found from the assumption that  $R_{\text{SPH}}$  is equal to the Roche lobe (RL) overflow radius,  $R_{\text{rlf}}$ , and using the approximation by Eggleton (1983). The initial orbital period,  $P_{\text{orb,ini}}$  is found assuming a Keplerian orbit. For the synchronized cases, the orbital period and separation are found at the moment when the RG overflows its Roche lobe (see §2.3 of Lombardi et al. 2011).

**Equations of state (EOS).** The standard EOS (SEOS) in StarSmasher is analytical and includes radiation pressure and ideal gas contributions. To take into account recombination energy, we need another prescription for the EOS. Because we evolve the specific internal energy  $u_i$  and density  $\rho_i$  for each particle (among other variables), we prefer an EOS that uses  $u_i$  and  $\rho_i$  as independent variables. However, such an analytical expression does not exist in simple form when we consider recombination/ionization of atoms. Therefore, we are bound to use a tabulated EOS (TEOS) which uses  $u_i$  and  $\rho_i$  to provide the gas pressure  $P_{\text{gas},i}$ , temperature  $T_i$ , specific entropy  $s_i$ , etc.

We use the MESA-EOS module to calculate such tables (see §4.2 of Paxton et al. 2011). The core of a RG is modeled as a point mass, and the rest of the star has uniform composition. Hence, only one table with a single set of composition for H, He, and metals needs to be generated for each RG. The tables that we generate operate in  $9.84 \leq \log u [\text{erg g}^{-1}] \leq 19.0$  and  $-14 \leq \log \rho [\text{g cm}^{-3}] \leq 3.8$ . When a particle has a density or specific internal energy outside the limits of our tables, we switch to the SEOS.

**Energy formalism.** The energy formalism compares the donor’s envelope binding energy  $E_{\text{bind}}$  with the orbital energy before,  $E_{\text{orb,ini}}$ , and after the CEE,  $E_{\text{orb,fin}}$  (Webbink 1984; Livio & Soker 1988):

$$E_{\text{bind}} = \alpha_{\text{bind}}(E_{\text{orb,fin}} - E_{\text{orb,ini}}) \equiv \alpha_{\text{bind}} \Delta E_{\text{orb}}. \quad (1)$$

Here  $\alpha_{\text{bind}}$  is the fraction of the released orbital energy used to expel the CE,  $0 \leq \alpha_{\text{bind}} \leq 1$ . The binding energy of the donor’s envelope, in its standard definition, is

$$E_{\text{bind}} = \sum_i m_i \left( \phi_i + \frac{3}{2} \frac{kT_i}{\mu_i m_H} + \frac{aT_i^4}{\rho_i} \right), \quad (2)$$

where  $m_i$ ,  $T_i$ ,  $\rho_i$ ,  $\phi_i$  and  $\mu_i$  are the mass, temperature, density, specific gravitational potential energy, and mean molecular mass, respectively, for each particle  $i$ . The constants  $k$ ,  $a$ , and  $m_H$  are the Boltzmann constant, radiation constant, and hydrogen atom mass, respectively, while  $\phi_i$  is calculated as in Hernquist & Katz (1989). Note that  $E_{\text{bind}}$  in its standard definition does not include recombination energy.

The binding energy of the donor’s envelope is frequently parameterized using a parameter  $\lambda$ , defined as (de Kool 1990)

$$\lambda \equiv -\frac{GM_{d,1}M_{env,1}}{E_{\text{bind}}R_{\text{rlf}}}. \quad (3)$$

Here  $G$  is the gravitational constant. For low-mass giants,  $\lambda$  is known to have a value close to one, and we obtain similar results.

We find the orbital energy of the binary system according to

$$E_{\text{orb}} = \frac{1}{2} \mu |\mathbf{V}_{12}|^2 + \sum_i \frac{1}{2} m_i \phi_i - \sum_j \frac{1}{2} m_j \phi_j^{\text{RL1}} - \sum_k \frac{1}{2} m_k \phi_k^{\text{RL2}}, \quad (4)$$

where  $\mu = M_1 M_2 / (M_1 + M_2)$  is the reduced mass, and  $\vec{V}_{12} = \vec{V}_1 - \vec{V}_2$  is the relative velocity of the two stars. The first term gives the orbital kinetic energy. The second term is the total gravitational energy of the binary, with the sum being over all particles  $i$  in the binary. The third and fourth terms correspond to the removal of the self-gravitational energy of the donor (the sum being over particles  $j$  in star 1) and of the WD (the sum being over particles  $k$  in star

2, initially only the WD), respectively: the remaining gravitational energy is then just the orbital contribution.

**Recombination energy.** In our treatment, the internal energy provided by the TEOS includes contributions from ideal gas, radiation, and the recombination energy for H, He, C, O, N, Ne, and Mg (see §4.2 of Paxton et al. 2011). The recombination energy can be extracted as

$$E_{\text{rec}} = \sum_i m_i \left( u_i - \frac{3}{2} \frac{kT_i}{\mu_i m_{\text{H}}} - \frac{aT_i^4}{\rho_i} \right) \equiv \alpha_{\text{rec}} \Delta E_{\text{orb}}, \quad (5)$$

where  $u_i$  is the SPH specific internal energy of particle  $i$ . Values of  $E_{\text{rec}}$ , as expected, scale well with the mass of the envelope. Note that here we introduce important new parameter,  $\alpha_{\text{rec}}$  – the ratio between the recombination energy and the released orbital energy.

**Total energy.** The initial total available energy,  $E_{\text{tot,ini}}$ , is

$$E_{\text{tot,ini}} = E_{\text{orb,ini}} + E_{\text{bind}} + E_{\text{rec}}. \quad (6)$$

This quantity is conserved during the evolution of all our models.

**Bound and unbound material.** For each particle, its total energy is defined as  $E_{\text{tot},i} \equiv 0.5m_i v_i^2 + m_i \phi_i + m_i u_i$ , where the first, second and third terms are the kinetic, potential, and internal energies, respectively. If the particle has negative total energy, it is bound to the binary. In this case, if the particle is located outside of either RL, the particle is in the circumbinary region. Accordingly, we classify the particles to be in (i) the *ejecta*,  $m_{\text{unb}}$  – the particles with positive energy, (ii) the *circumbinary*,  $m_{\text{cir}}$  – the matter bound to the binary but outside of the two RLs, and (iii) *binary*,  $m_{\text{bin}}$  – the particles are inside either of the two RLs.

The total energy of the unbound material at infinity is computed when the unbound mass is in a steady state after the CEE:

$$E_{\text{tot,unb}}^{\infty} = \sum_i E_{\text{tot},i}^{\text{unb}} = -\alpha_{\text{unb}}^{\infty} \Delta E_{\text{orb}}. \quad (7)$$

Here we introduce  $\alpha_{\text{unb}}^{\infty}$  – the energy taken away by the unbound material in units of the released orbital energy. Note that in the standard energy formalism this quantity is always assumed to be zero.

**Angular momentum budget.** We calculate the orbital angular momentum

$$\vec{J}_{\text{orb}} \equiv \mu \vec{R}_{12} \times \vec{V}_{12}, \quad (8)$$

where  $\vec{R}_{12} = \vec{R}_1 - \vec{R}_2$  is the displacement from star 2 to star 1. We note that the magnitude  $J_{\text{orb}} = |J_{\text{orb,z}}|$ , where the  $z$ -direction is perpendicular to the orbital plane. An outcome of a CEE can be characterized by how much orbital angular momentum is lost. We provide the  $\gamma$ -parameter (Nelemans et al. 2000; Nelemans & Tout 2005) as a way of quantifying angular momentum loss in our simulations:

$$\gamma = \frac{M_1 + M_2}{M_{\text{unb}}} \frac{J_{\text{orb,ini}} - J_{\text{orb,fin}}}{J_{\text{orb,ini}}}. \quad (9)$$

### 3 FORMATION OF A DWD THROUGH A CEE

**Comparison between the two EOSs.** We compare the results of simulations with our two different EOSs using the model 1.5RG2N. In both cases, the initial relaxed stars have SPH profiles that match very well the 1D stellar profiles for pressure, density, and gravitational potential. However, this is not the case for the specific internal energy  $u$  (see Figure 1): clearly only the TEOS model matches the desired 1D stellar profile. As expected, the mismatch between the relaxed profile with SEOS and the stellar one is indeed due to neglecting recombination energy.

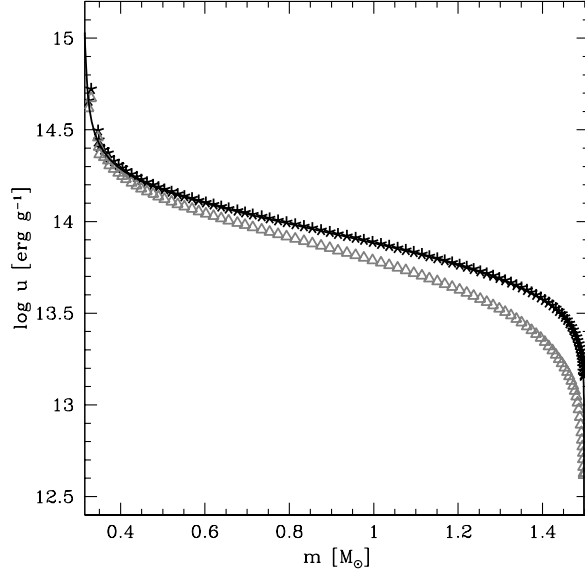


**Figure 1.** Specific internal energy  $u$  profiles for the model 1.5RG2N. The black asterisks and gray triangles correspond to relaxed  $u$  profiles for TEOS and SEOS, respectively. The black solid line corresponds to the  $u$  profile from the stellar code.

We find that the SEOS fails to unbind the envelope in our CE simulations. Only about 50% of the envelope becomes unbound: the circumbinary matter does not interact with the formed binary at all, making it impossible to eject the entire envelope. This result is consistent with the findings of previous studies (Passy et al. 2012; Ricker & Taam 2012). On the other hand, the TEOS simulation clearly makes use of the recombination energy and ejects the envelope entirely. For all other models presented in the *Letter*, we use the TEOS.

**Masses.** At the end of the simulations, we form a binary consisting of  $M_1$  and  $M_2$  (see Table 2 for all the outcomes). The unbound material  $M_{\text{unb}}$  is at least 99.8% of the initial envelope. A few, usually less than 10, SPH gas particles remain bound to the newly formed binary, been bound to either the newly formed WD, or the old WD. This explains why  $M_1$  can be slightly larger than  $M_{\text{c},1}$ , and similarly why  $M_2$  can exceed slightly  $0.36M_{\odot}$ . There is no circumbinary envelope left in all simulations with the TEOS. In all our simulations, the final mass ratio  $q$  ranges between 0.88 – 0.90, consistent with the observational error for WD 1101+364.

**Energies.** The total energy at the end of the simulation is distributed in the “binding” energy of the gas bound to the binary,  $E_{\text{bound}}$ , the final orbital energy of the binary,  $E_{\text{orb,fin}}$ , and the total energy of the unbound material at infinity,  $E_{\text{tot,unb}}^{\infty}$ :

$$E_{\text{tot,fin}} = E_{\text{orb,fin}} + E_{\text{bound}} + E_{\text{tot,unb}}^{\infty}. \quad (10)$$

We have compared the initial and the final total energies and found that the error is less than 0.11% in all our simulations.

$E_{\text{tot,unb}}^{\infty}$  is composed of  $E_{\text{kin,unb}}^{\infty}$ ,  $E_{\text{int,unb}}^{\infty}$ ,  $E_{\text{pot,unb}}^{\infty}$  – the kinetic, internal and potential energies of the unbound material, respectively. We note that  $E_{\text{kin,unb}}^{\infty}$  is the dominant energy in the unbound material, though the internal energy of the unbound material at the end of the simulations is also non-negligible (see Table 2).

We present  $E_{\text{bound}}$  for completeness, but the fate – accretion or ejection – of the several particles that remain bound to the binary can not be resolved by the numerical method we use; on the

**Table 2.** Energies and masses

Model	$M_{\text{unb}}$	$M_1$	$M_2$	$E_{\text{kin,unb}}^{\infty}$	$E_{\text{int,unb}}^{\infty}$	$E_{\text{pot,unb}}^{\infty}$	$E_{\text{tot,unb}}^{\infty}$	$E_{\text{orb,fin}}$	$E_{\text{bound}}$	$E_{\text{tot,fin}}$	$\Delta E_{\text{orb}}$
1.0RG0N	0.663	0.322	0.360	3.645	0.473	-0.025	4.093	-10.992	-0.615	-7.514	-9.874
1.0RG1N	0.663	0.322	0.360	4.123	0.295	-0.015	4.403	-11.278	-0.582	-7.457	-10.220
1.0RG2N	0.663	0.322	0.360	4.081	0.543	-0.024	4.600	-11.469	-0.531	-7.400	-10.490
1.2RG2N	0.872	0.323	0.360	4.604	0.629	-0.041	5.192	-15.504	-0.639	-10.951	-14.159
1.4RG2N	1.079	0.319	0.360	6.790	0.907	-0.094	7.603	-22.911	-0.005	-15.313	-21.196
1.5RG2N	1.178	0.319	0.361	6.089	0.917	-0.096	6.910	-25.484	-0.026	-18.600	-23.469
1.5RG2NP	1.178	0.320	0.360	7.415	1.407	-0.159	8.663	-26.969	-0.366	-18.665	-24.958
1.6RG2N	1.274	0.323	0.362	5.623	1.812	-0.440	6.995	-27.741	-0.244	-20.990	-25.584
1.6RG0S	1.274	0.323	0.362	5.603	1.692	-0.381	6.914	-27.228	-0.309	-20.623	-24.987
1.7RG2N	1.370	0.323	0.366	5.854	2.042	-0.417	7.479	-33.692	-0.715	-26.928	-31.073
1.7RG0S	1.373	0.323	0.363	5.032	2.061	-0.610	6.483	-32.417	-0.466	-26.400	-29.723
1.8RG2N	1.478	0.318	0.362	8.333	1.675	-0.371	9.637	-52.873	-0.171	-43.407	-48.961

$M_{\text{unb}}$ ,  $M_1$ , and  $M_2$  are the unbound, stripped RG core and old WD, in  $M_{\odot}$ .  $E_{\text{kin,unb}}^{\infty} = \sum_i m_i^{\text{unb}} v_i^2/2$ ,  $E_{\text{int,unb}}^{\infty} = \sum_i m_i^{\text{unb}} u_i$ ,  $E_{\text{pot,unb}}^{\infty} = \sum_i m_i^{\text{unb}} \phi_i$ , and  $E_{\text{tot,unb}}^{\infty}$  are kinetic, internal, potential and total energies, respectively, for the unbound material.  $E_{\text{orb,fin}}$  is the orbital energy after the CEE.  $E_{\text{bound}}$  is the total energy of the particles that remained bound to the binary.  $E_{\text{tot,fin}}$  is the total energy of all the particles. All energies are in  $10^{46}$  erg.

timescale of our simulation they stay in an orbit within the RL of their stars. This energy includes the kinetic, internal, potential and recombination energies for these several SPH gas.

We should clarify that  $E_{\text{orb,fin}}$  does not have to match with the two-body approximation, namely  $E_{\text{orb}} = -GM_1M_2/(2a_{\text{orb}})$ . In the latter, the potential assumes a form  $\phi \propto 1/r$ , while our code includes the softened form as described in the appendix of Hernquist & Katz (1989). When the separation between the two SPH special particles is more than two smoothing lengths, the potential reduces to the Keplerian form. However, this separation is less than two smoothing lengths for the point particles after the CEE, and the potential is softened accordingly. The difference in orbital energy between the two methods varies from about 3% (for 1.0RG0N) to 14% (for 1.8RG2N), with the Keplerian values being closer to zero. The initial orbital energy, given by Equation 4, is the same as in the two-body approximation.

Because energy is well conserved, we can equate Equations 6 and 10. For that, we also use Equations 1, 5, and 7. If we neglect  $E_{\text{bound}}$ , we can re-write the conservation of energy in fractions of the change in the orbital energy:

$$\alpha_{\text{bind}} + \alpha_{\text{rec}} + \alpha_{\text{unb}}^{\infty} \approx 1. \quad (11)$$

We find that this is indeed the case in our simulations (see Table 3), and that the deviation from 1 is due to  $E_{\text{bound}}$ : the maximum deviation occurs in 1.0RG0N ( $\sim 7.8\%$ ) and the minimum in 1.4RG2N ( $\sim 0.03\%$ ). Note that if  $\alpha_{\text{rec}} = \alpha_{\text{unb}}^{\infty} = 0$ , the previous equation reduces to the standard energy formalism. However, values of both  $\alpha_{\text{rec}}$  and  $\alpha_{\text{unb}}^{\infty}$  are non-negligible and comparable to  $\alpha_{\text{bind}}$ . We emphasize that previously it had been anticipated only that  $\alpha_{\text{bind}}$  is somewhat less than 1, and we provide new improved constraints. Unfortunately, this is not yet a final solution of the problem as  $\alpha_{\text{unb}}^{\infty}$  can not be easily predicted for any system—a subject of our future studies.

**Orbital angular momenta.** We find that the ejected material takes away more than 90% of the initial angular momentum of the binary. Values of  $\gamma$  vary between 1.42 and 1.87. This large range of values unfortunately does not allow the obtained values of  $\gamma$  to be useful for predicting the final parameters in a population synthesis for all possible DWD systems (for details, see Ivanova et al. 2013).

**Final orbital parameters.** We find the final orbital separation as  $a_{\text{orb,fin}} = (r_a + r_p)/2$ , where  $r_p$  is the periastron, and  $r_a$  is

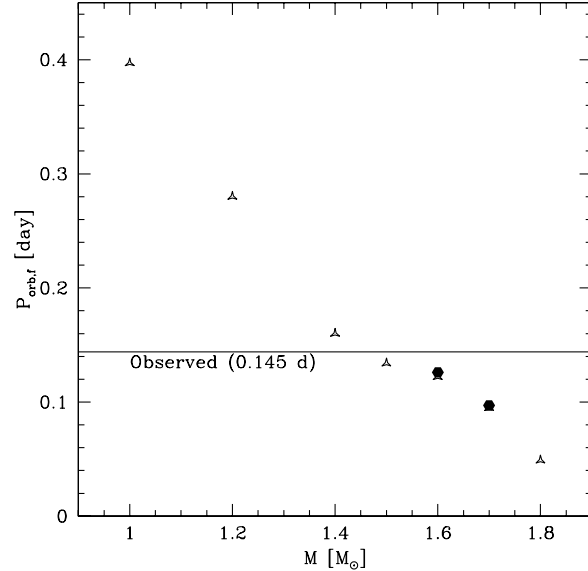


**Figure 2.** Final orbital periods versus initial mass of a RG. Triangles represent non-synchronized RGs, and circles represent synchronized RGs. Note: to compare alike cases, we show only the  $\eta = 2$  cases with our standard resolution. Different  $\eta$ 's give similar outcomes (see Table 3).

the apastron. We ensure that these two quantities,  $r_p$  and  $r_a$ , do not change with time at the moment when we extract them from the simulations. We calculate the final orbital period  $P_{\text{orb,fin}}$  of the binary from Kepler's third law and the eccentricity of the post-CE orbit as  $e = (r_a - r_p)/(2a_{\text{orb,fin}})$ . The latter is small in all the models, showing that post-CE orbits are almost circular (in previous studies, where the ejection of the CE was incomplete, the final eccentricity was larger, 0.08 or more, e.g. Ricker & Taam 2012).

Figure 2 shows the final orbital periods plotted versus initial RG. We see that, as expected, the more massive the star is, the tighter the orbit gets. We find also that the final orbital period for the non-synchronized and synchronized cases are very similar (for the final state of the binary system, the only change due to synchronization was observed for the final eccentricity, albeit final eccentricity



**Table 3.** Orbital parameters

Model	$J_{\text{orb,ini}}$	$J_{\text{orb,fin}}$	$\gamma$	$r_p$	$r_a$	$a_{\text{orb,fin}}$	$P_{\text{orb,fin}}$	$e$	$\alpha_{\text{bind}}$	$\alpha_{\text{rec}}$	$\alpha_{\text{unb}}^\infty$
1.0RG0N	14.340	1.188	1.861	2.015	2.115	2.065	0.416	0.024	0.855	-0.208	0.431
1.0RG1N	14.741	1.168	1.868	1.965	2.074	2.020	0.403	0.027	0.827	-0.201	0.431
1.0RG2N	15.119	1.157	1.873	1.947	2.036	2.000	0.397	0.022	0.808	-0.197	0.440
1.2RG2N	16.262	0.987	1.670	1.520	1.532	1.526	0.264	0.004	0.871	-0.192	0.367
1.4RG2N	17.116	0.759	1.557	1.070	1.089	1.080	0.158	0.009	0.800	-0.159	0.359
1.5RG2N	17.062	0.709	1.512	0.953	1.003	0.978	0.134	0.026	0.879	-0.172	0.294
1.5RG2NP	17.062	0.719	1.511	0.891	0.924	0.908	0.122	0.018	0.815	-0.148	0.347
1.6RG2N	17.685	0.678	1.479	0.880	0.948	0.914	0.122	0.037	0.893	-0.157	0.273
1.6RG0S	17.392	0.690	1.477	0.912	0.947	0.930	0.126	0.019	0.895	-0.160	0.277
1.7RG2N	17.151	0.610	1.449	0.746	0.771	0.758	0.092	0.016	0.922	-0.140	0.241
1.7RG0S	16.953	0.624	1.444	0.776	0.791	0.784	0.097	0.009	0.942	-0.146	0.218
1.8RG2N	14.932	0.446	1.417	0.464	0.493	0.479	0.047	0.030	0.902	-0.096	0.197

The orbital angular momentum  $J_{\text{orb,ini}}$  and  $J_{\text{orb,fin}}$  for the initial and final binary, respectively, in units of  $10^{52} \text{ g cm}^2 \text{ s}^{-1}$ . The parameter  $\gamma$  is defined in Eq. 9. The closest and farthest orbital separations are  $r_p$  and  $r_a$ , respectively, while  $a_{\text{orb,fin}}$  is the semimajor axis (all in  $R_\odot$ ). The orbital period  $P_{\text{orb,fin}}$  is given in days, and  $e$  is the eccentricity of the orbit. The energy fractions  $\alpha_{\text{bind}}$ ,  $\alpha_{\text{rec}}$ , and  $\alpha_{\text{unb}}^\infty$  are defined in Eq. 1, Eq. 5, and Eq. 7, respectively.

is small in all the cases). We conclude that our best progenitor for WD 1101+364 is a  $1.4 - 1.5M_\odot$  RG.

#### 4 CONCLUSIONS

To understand the energy budget during a CEE leading to a DWD formation, we perform non- and synchronized 3D hydrodynamic simulations with two EOSs. We confirm that taking into account recombination energy leads to a full ejection of the RG's envelope and the formation of a non-eccentric binary system, whilst if we do not take recombination energy into account, we obtain result similar to previous studies and only half of the RG's envelope is ejected. The most important consideration appears not to be the value of the available recombination energy, but where and when this energy is released. Indeed, ionized material forms the circumbinary envelope initially. Recombination then takes places there, while the circumbinary envelope continues to expand. This results in the ejection of the circumbinary envelope and effectively of all the common envelope material. If instead the recombination energy had been released too early, the simulations would have ended up with unexpelled circumbinary envelope as in previous studies. In addition, we find that considering a complete synchronization versus non-synchronized case does not change noticeably the final results.

We introduce a modification of the standard energy formalism (Webbink 1984; Livio & Soker 1988), with the parameters describing the use of the recombination energy and the unbound material energy. The first one can be found from initial stellar models, but the latter requires 3D simulations. For our set of models,  $\alpha_{\text{unb}}^\infty$  has values from about 0.2 to about 0.44. However to generalize the result and make it useful for population synthesis one needs to make a thorough parameter study; this is the subject of our future studies.

As expected, we find that the more massive the parent RG star is, the tighter the final orbit gets. We do not find that the initial synchronization affects the final period but instead only changes the energy and angular momentum carried away by the ejecta, presumably shaping the post-CE nebula. We also find that our binaries end up with an eccentricity smaller than 0.04—a result that has been expected theoretically but not yet produced in simulations.

We applied our method to the case of WD 1101+364, a well-known DWD (see Marsh 1995). We inferred that its progenitor bi-

nary could have been composed of a  $1.4 - 1.5M_\odot$  RG and a  $0.36M_\odot$  WD companion, with  $P_{\text{orb,ini}} \approx 31 - 33$  days.

#### ACKNOWLEDGMENTS

JLAN acknowledges CONACyT for its support. NI thanks NSERC Discovery and Canada Research Chairs Program. JCL is supported by National Science Foundation (NSF) grant number AST-1313091. This research has been enabled by the use of computing resources provided by WestGrid and Compute/Calcul Canada.

#### REFERENCES

- de Kool M., 1990, ApJ, 358, 189
- Eggleton P. P., 1983, ApJ, 268, 368
- Gaburov E., Lombardi Jr. J. C., Portegies Zwart S., 2010, MNRAS, 402, 105
- Glebbeek E., Pols O. R., Hurley J. R., 2008, A&A, 488, 1007
- Han Z., Podsiadlowski P., Eggleton P. P., 1994, MNRAS, 270, 121
- Han Z., Podsiadlowski P., Maxted P. F. L., Marsh T. R., Ivanova N., 2002, MNRAS, 336, 449
- Hernquist L., Katz N., 1989, ApJS, 70, 419
- Ivanova N., et al. 2013, A&A Rev., 21, 59
- Livio M., Soker N., 1988, ApJ, 329, 764
- Lombardi Jr. J. C., et al. 2011, ApJ, 737, 49
- Lucy L. B., 1967, AJ, 72, 813
- Marsh T. R., 1995, MNRAS, 275, L1
- Nandez J. L. A., Ivanova N., J. C. Lombardi J., 2014, The Astrophysical Journal, 786, 39
- Nelemans G., Tout C. A., 2005, MNRAS, 356, 753
- Nelemans G., Verbunt F., Yungelson L. R., Portegies Zwart S. F., 2000, A&A, 360, 1011
- Paczyński B., Ziółkowski J., 1968, Acta Astron, 18, 255
- Passy J.-C., et al. 2012, ApJ, 744, 52
- Paxton B., et al. 2011, ApJS, 192, 3
- Ricker P. M., Taam R. E., 2012, ApJ, 746, 74
- Roxburgh I. W., 1967, Nature, 215, 838
- Sandquist E. L., et al. 1998, ApJ, 500, 909
- Webbink R. F., 1984, ApJ, 277, 355